iJRASET
International Journal For Research in Applied Science and Engineering Technology

INTERNATIONAL JOURNAL FOR RESEARCH

IN APPLIED SCIENCE & ENGINEERING TECHNOLOGY

Volume: 8 **Issue:** XI **Month of publication:** November 2020

DOI: https://doi.org/10.22214/ijraset.2020.32287

www.ijraset.com

Call: 08813907089 | E-mail ID: ijraset@gmail.com

International Journal for Research in Applied Science & Engineering Technology (IJRASET)
ISSN: 2321-9653; IC Value: 45.98; SJ Impact Factor: 7.429
Volume 8 Issue XI Nov 2020- Available at www.ijraset.com

CFD Simulation of Valves in Process Industries

Harshawardhan Kulkarni
Institute of chemical technology, India

Abstract: ***Flow control valves are commonly used to regulate the flow in the process and petroleum industries. The valves work by either opening or closing in its entire or partial capacity in response to certain criteria. The flow through the control valves depend on the % opening and upstream pressure. The flow rate is not linear with % opening as well as the pressure drop significantly changes with the valve opening. Computational fluid dynamics has been increasingly used in the study of complex piping networks. In the present work, detailed study of orifice plate, ball, globe and gate valves has been carried out using CFD. The pressure drop data, volume average dissipation rate and profiles of flow pattern, turbulent kinetic energy as well as rate of dissipation of turbulent kinetic energy have been used as model validation parameter to select appropriate turbulence model. Detailed flow patterns at the downstream of these components, turbulent kinetic energy as well as rate of dissipation of turbulent kinetic energy on the pipe wall have been quantified. Based on the rate of dissipation and analogy of mass and momentum transfer we have quantified the rate of erosion at the downstream of the component. The validated CFD model can be used for sensitivity study of operating parameters to decide the operation window in terms of % opening and possible replacement frequency.***

Keywords: Gate valve, globe valve, ball valve, orifice, CFD

I. INTRODUCTION

In a typical petroleum complex and thermal/nuclear power stations, thousands of valves are used for variety of applications including controlling various parameters. Medium and fine chemical industries also employ various flow control devices to regulate flow of reactants, products and utilities. These valves offer pressure drop in the system to control the flow. The increase in pressure drop reflects in dissipation of energy and leads to Reynolds stresses exerted on piping structures. Flow control valves such as Globe, Gate and Ball valves are routinely used in chemical process industries. Gate and Ball valves are mainly used as on/off valves whereas globe valve is used for precise flow control. These control valves offer significant pressure drop as well as the flow patterns in the vicinity of these devices are complex. The pressure drop is significantly higher under partially open conditions and the wall shear stress is significantly higher at the downstream locations and can induce flow assisted corrosion in nuclear/thermal power plants at high pressure and temperature conditions. Shirazi N.T et al. carried CFD simulations of ball valve at several opening angles. They predicted pressure drop across the valve and observed that as the opening of the valve decreases these vortices grow and may cause more pressure drop[1]. Moujaes S.F et al. simulated ball valve at various opening angles and Reynolds numbers. They compared the head loss coefficient with the ASHRAE database and observed reasonably good predictions. The head loss coefficient values showed strong correlation with the degree of valve opening and did not influence much by the Re number variations[2]. Similar analysis of gate valve has been carried out by Augusto P.E.D et al. and Choudhary S et al.. They compared the head loss coefficient with literature reported values[3,4]. Fluid flow behaviour through the gate valve showed the flow recirculation and stagnant areas[5]. Tang Y et al. Studied the solid particle erosion in the gate valves using two-way Eulerian-Lagrangian [6].

II. CFD SIMULATION OF FLOW BALL VALVE

Ball valves can be used in a variety of applications and markets, such as transmission and storage, gas processing, industrial, and many more. Mainly these valves are used for on/off applications rather than precise control. It is a device having a spherical closure unit that provides on/off control of flow. Schematic of ball valve is shown in Figure 2.1. The sphere has a port, also known as a bore, through the center. When the valve is positioned such that the bore is aligned in the same direction as the pipeline, it is in open position and fluid can flow through it. When rotated 90 degrees, the bore becomes perpendicular to the flow path, meaning the valve is closed and the fluid cannot pass through. The most common ball valves are considered to be two-way, which allows flow to travel linearly from the inlet to the exit. There are two types of ball valves in operation. One is full-port ball valve – A full-port, also known as a full-bore, ball valve has a bore internal diameter (ID) approximately equal to the pipeline ID and other is Reduced-Port Ball Valve – A reduced-port, also known as a reduced-bore, ball valve is a valve in which the bore is reduced to one or two nominal sizes lower.

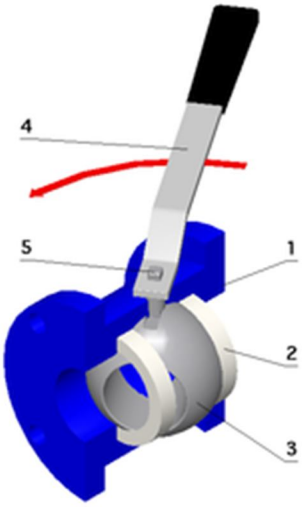

Figure 2.1: Cut-away view of ball valve components: 1) body 2) seat 3) floating ball 4) lever handle 5) stem

It is necessary to understand the energy dissipation and shear offered by the ball valve at different opening conditions. This information will be useful to quantify the wear rate in practice. This study has been undertaken by carrying of simulation of ¾ inch ball valve at different % opening (namely full, 75%, 50% and 25%) and pipe Reynolds number (10000, 25000 and 50000). The flow patterns inside the valves and at the downstream are complex and hence it is necessary to select appropriate turbulence model. Reduction in the cross-section area at the valve causes increase in velocity and reduction in pressure. This pressure – velocity conversion is quite complex and such energy distribution cannot be captured by simplified modelling approaches. Hence in this work, we have carried out simulation with standard k-ε model, SST k-ω model and Reynolds stress model (RSM). Standard k-ε models are very popular and are used to study flow systems where turbulence in bulk flow is analyzed. SST k-ω models are used in case of swirling flows, flows with recirculation etc. The RSM is a very generalized RANS model and can capture majority of flow features, however it is computationally expensive compared to other RANS models. RSM is found to capture many complex flow cases such as fluid jets hitting walls, where significant energy redistribution in the flow takes place. Hence it was thought necessary to first compare the results of all the three RANS model and the carry out detailed study with the turbulence model which gives reasonable predictions and if possible faster results. Table 3.1 shows the results obtained by various turbulence model for different flow conditions, it can be seen that the predictions by standard k-e model and k-ω model are significantly higher compared to RSM model. RSM model predictions were found to be in agreement with the literature reported head loss coefficient data. Hence rest of the studies are carried out using RSM.

Table 2.1: Simulation results of Ball valve

Valve	Model	% Opening	Re	ε, m^2/s^3	Δp, Pa
Ball	k-ε	25	10k	126.9	262850
Ball	k-ε	50	10k	5.706	11818
Ball	k-ε	75	10k	0.9975	2066
Ball	k-ε	100	10k	0.296	613
Ball	k-ε	100	25k	3.299	6833
Ball	k-ε	100	50k	23.77	49235
Ball	RSM	25	10k	87.76	12647
Ball	RSM	50	10k	4.352	9014
Ball	RSM	75	10k	0.8185	1695

Ball	RSM	100	10k	0.2472	512
Ball	RSM	100	25k	3.003	6220
Ball	RSM	100	50k	21.42	44367
Ball	k-ω	25	10k	110.71	229351
Ball	k-ω	50	10k	4.3769	9065
Ball	k-ω	75	10k	0.863	1787
Ball	k-ω	100	10k	0.1974	408
Ball	k-ω	100	25k	3.138	6944
Ball	k-ω	100	50k	17.32	35875

Figure 2.2 shows the velocity magnitude at Reynolds number of 10000 through ball valves at different opening conditions. It can be seen that for a reduced ball valve, under fully open condition, the velocity pattern in not much affected whereas when we start throttling the valve, the flow pattern becomes quite complex and the effect of valve is experienced till L/D of 4 at the downstream of the valve. The flow pattern becomes increasingly chaotic up to 25% opening condition. Similar effect can also be observed in velocity vector plots (Figure 2.3).

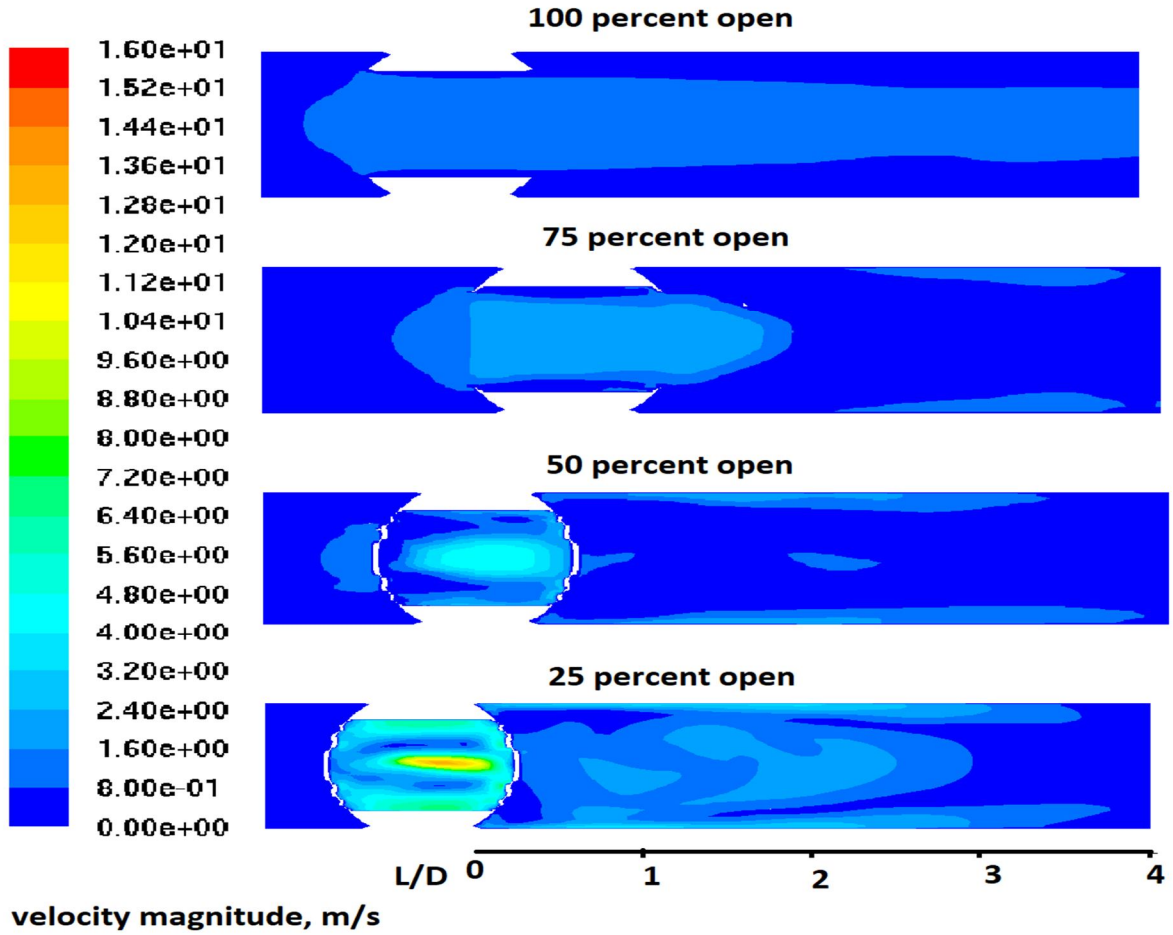

Figure 2.2: Velocity magnitude through ball valve at different % opening

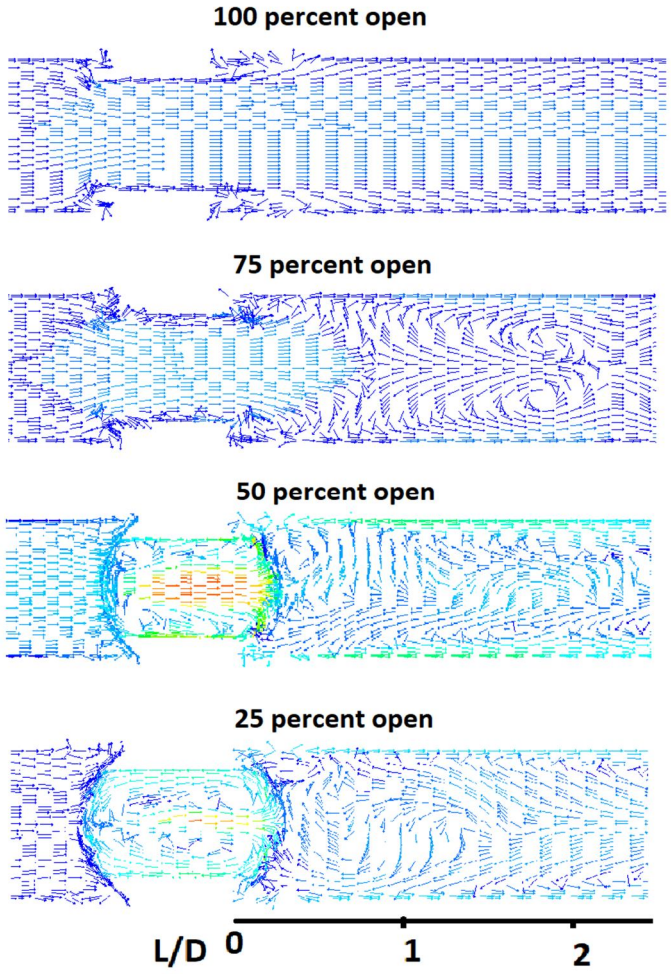

Figure 2.3: Velocity vector through ball valve at different % opening

Figure 2.3 shows that at fully open conditions streamlines are not affected. With throttling up to 75 % opening, a flow recirculation starts at L/D of 2, which eventually starts at just downstream of the valve (L/D = 0) at 25 % opening. One of the major turbulence parameter is turbulent kinetic energy (TKE). This is the amount of energy extracted from the mean flow and utilized in the enhancement of transport rates in the system. This is the energy available with the turbulent eddies in the system. Figure 2.4 shows the TKE plot for ball valve at different % opening. It can be seen that with valve closure, the turbulence in the system is increasing exponentially. The TKE value at the downstream of ball valve is in the range of 0.001, 0.007, 0.3 and 20 m^2/s^2 for fully open, 75% open, 50% open and 25% open conditions. At 25% opening, we can see a low TKE region at L/D of about 0.75 to 1.25 at the centre line, which is an indicator of sort of dead zone in the system where flow stagnation can be observed. At 25% opening condition, the TKE value close to the wall is about 0.4 m^2/s^2 which is significantly higher than fully open condition (in the range of 0.007 m^2/s^2). This very high TKE magnitude is an indicator of velocity fluctuations close to the wall, leading to its wear and erosion. Another turbulence parameter of importance is the rate of dissipation of turbulent kinetic energy (ε). The rate of dissipation of TKE is shown in Figure 2.5 on the pipe wall. The dissipation on the pipe wall was found to increase from almost 2.5 to 630 from fully open to 25% opening condition. The dissipation rate is directly related with the mass transfer and can be estimated using theories of turbulence. One such popular theory is small eddy model which is proposed by Lamant and Scott (1968) and Banerjee et al. (1970). The mass transfer coefficient is proportional to $k_L = \sqrt{D_A}\left(\frac{\epsilon}{\nu}\right)^{\frac{1}{4}}$, where D_A is diffusivity of solute and kinematic viscosity ν is in the range of 1.7×10^{-7} m^2/s. Using these values and small eddy model it can be seen that the mass transfer coefficient at wall will be 0.008 m/s and 0.033 m/s at fully open and 25% open condition, respectively. It can be seen that the mass transfer rate at the wall increases by 4 times, which means that the component life will reduce by four times.

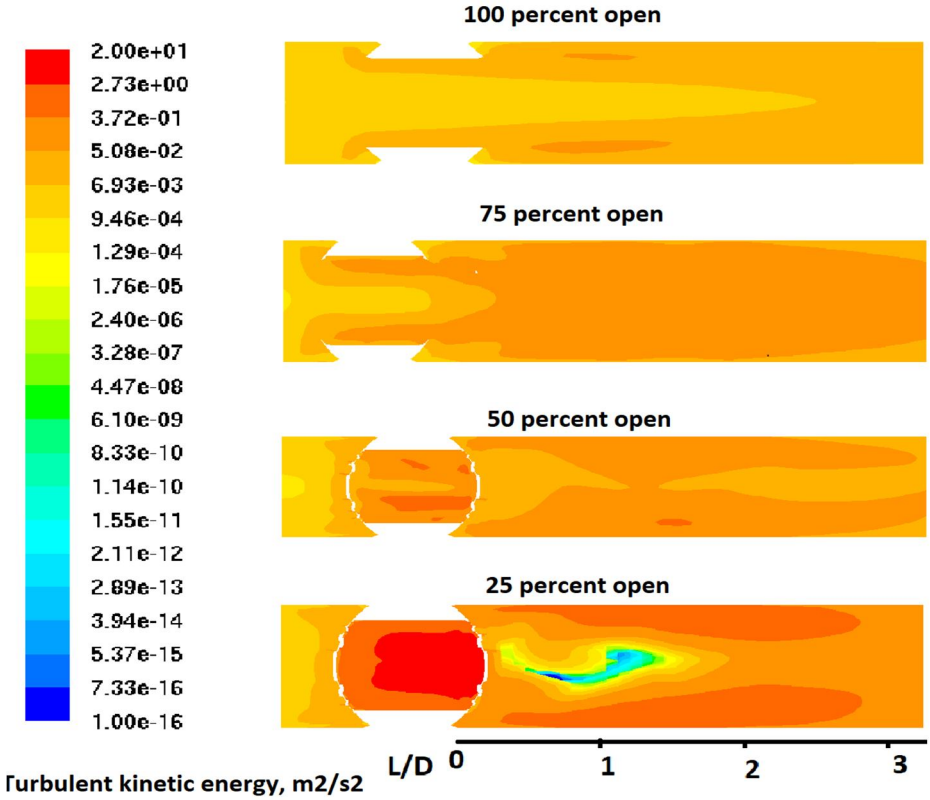

Figure 2.4: TKE through ball valve at different % opening

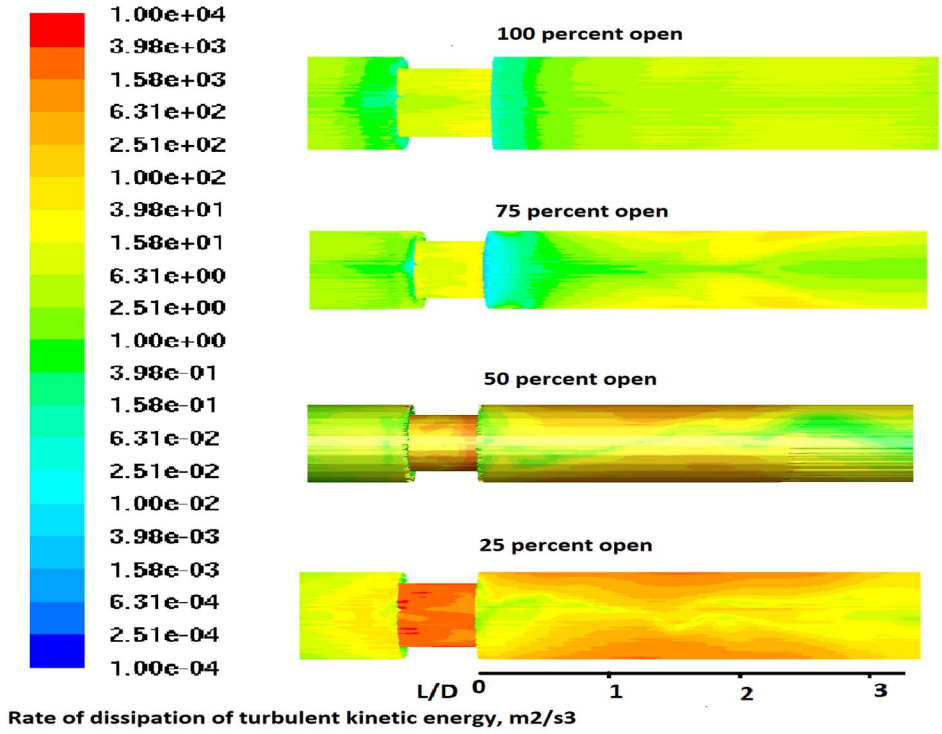

Figure 2.5: Rate of dissipation of TKE through ball valve at different % opening on the pipe wall

III. CFD SIMULATION OF GATE VALVE

Gate valves are widely used for all types of applications and are suitable for both above-ground and underground installation. Gate valves are designed for fully open or fully closed service. They are installed in pipelines as isolating valves and are rarely used as control or regulating valves. Gate valve consists of one gate or wedge and it will control the fluid flow. Shape of gate or wedge of gate valve will be a type of flat circular plate or rectangular plate. Sometimes, gate or wedge is also termed as disc of gate valve. There will be one handle wheel, as shown in Figure 3.1, with valve which is used to open and close the gate valve. When handle wheel will be rotated, it will move the gate or wedge in upward or downward direction across the line of fluid flow. Gate valve has two sections: Bottom section will be connected with the inlet line and outlet line with the help of flanges and upper section of gate valve will consist with the gate and stem. Handle wheel and gate will be attached with this stem with the help of pin assemble or screw assemble.

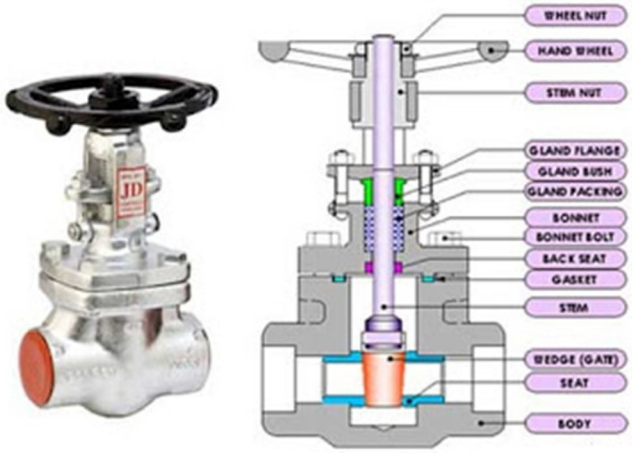

Figure 3.1: Internal structure of Gate Valve (Source: http://www.hkdivedi.com/2016/05/gate-valve-working-principle.html)

The working of the Gate Valve is as follows (Figure 3.2): When handle wheel will be rotated in clockwise direction, steam and gate will move in downward direction across the fluid flow line and gate will be tightly located between the two seats. Hence there will not be any leakage of fluid through the valve once valve is closed completely. The Gate valve offers resistance to the flow by partially closing the flow cross sectional area and will have similar complexities as that of orifice. The flow will involve dead zone at upstream and downstream of gate as well as strong variations in velocity streamlines. Figure 3.3 shows the velocity vectors across the gate valve at different % opening conditions are pipe Reynolds number of 10000. It can be seen that the recirculation zone is up to L/D of 4 irrespective of % opening (75 to 25 % opening condition). Figure 3.4 shows the velocity magnitude in the system and it can be seen that at constant flow condition, large amount of flow in pumped through the narrow opening for 25 % opening condition and the velocity profile do not get streamlined after L/D of 3 (like other cases), instead it can be observed that the streamlines become discontinuous and might originate to secondary flows in the system.

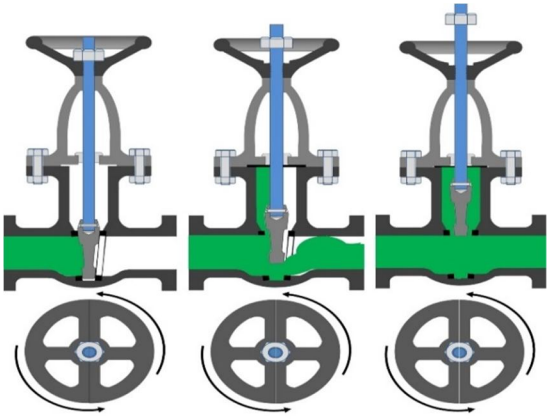

Figure 3.2 Working principle of Gate Valve

(Source: http://www.hkdivedi.com/2016/05/gate-valve-working-principle.html)

ISSN: 2321-9653; IC Value: 45.98; SJ Impact Factor: 7.429
Volume 8 Issue XI Nov 2020- Available at www.ijraset.com

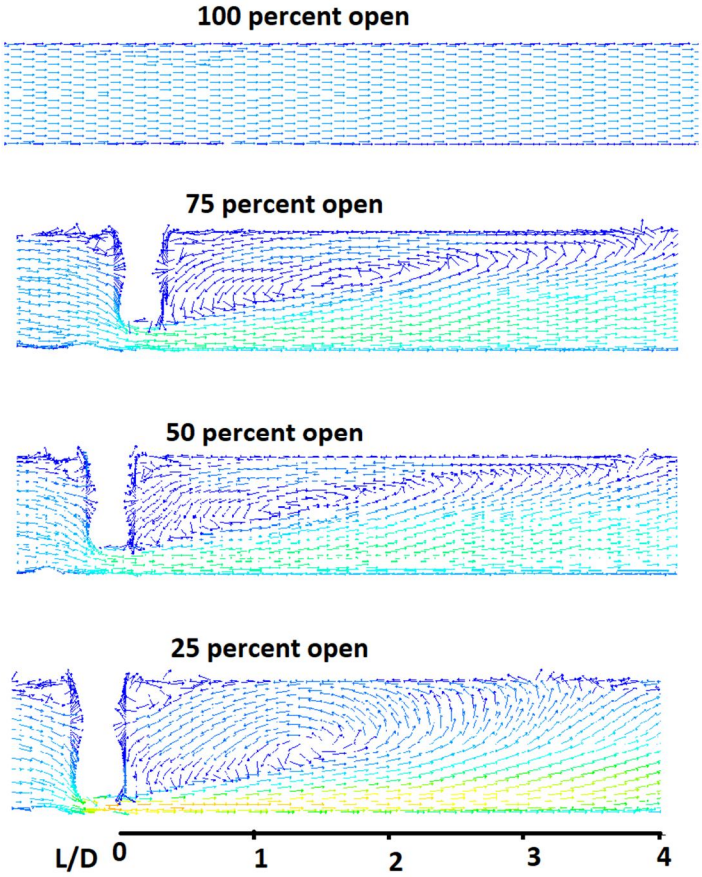

Figure 3.3: Velocity vectors through the Gate valve

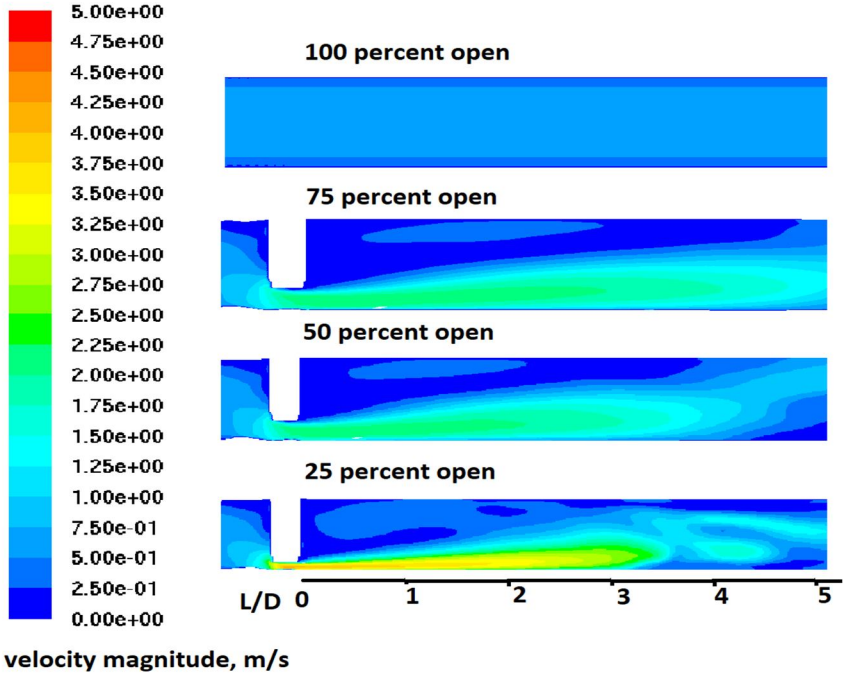

Figure 3.4: Velocity magnitude through the Gate valve

ISSN: 2321-9653; IC Value: 45.98; SJ Impact Factor: 7.429
Volume 8 Issue XI Nov 2020- Available at www.ijraset.com

Figure 3.5 shows the turbulent kinetic energy plot in the system for various opening conditions. The turbulent kinetic energy is almost constant close to the wall in the range of 0.004 m^2/s^2 for all % opening (fully open to 25 % opening condition). However, in the central zone, TKE is in the range of 0.025 m^2/s^2 for 50 and 75% opening condition and almost 0.2 m^2/s^2 for 25% opening condition. The turbulent intensity which is defined as $\sqrt{TKE}/u_{avg}$ is about 29% for 50 and 75% opening and 84% for 25% opening. Hence it can be seen that the highly energetic turbulent eddies start forming with the closure of gate valve. The characteristic sizes will be proportional to the % valve opening. Figure 3.6 shows the dissipation rate of turbulent kinetic energy. It can be seen that in case of 50 and 75% opening, the dissipation rate is in the range of 200 to 500 m^2/s^3 on the wall just downstream of the valve up to L/D of 0.5. In case of 25% opening condition, the dissipation rates vary from 3500 m^2/s^3 (at L/D of 0.5) to almost 200 m^2/s^3 (at L/D of 3). Using small eddy model, just downstream of gate valve in case of 50 and 75% opening, the wall mass transfer will be in the range of 0.025 to 0.032 m/s and for 25% opening condition it is 0.051 m/s. If we compare these results with ball valve at similar opening, the wear rates are almost four times at 50 and 75% opening condition and just less than twice for 25% opening condition.

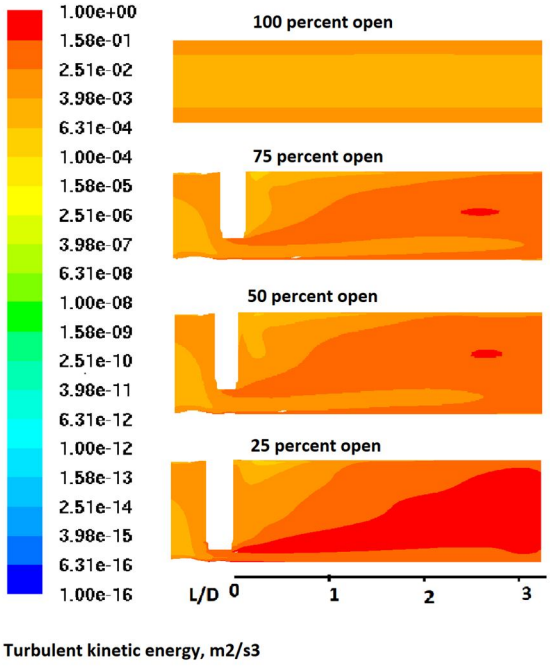

Figure 3.5: Turbulent kinetic energy profile through Gate valve

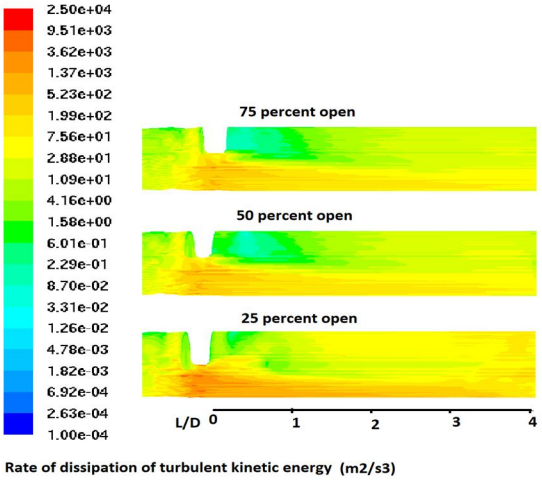

Figure 3.6: Turbulent kinetic energy profile through Gate valve

ISSN: 2321-9653; IC Value: 45.98; SJ Impact Factor: 7.429
Volume 8 Issue XI Nov 2020- Available at www.ijraset.com

IV. CFD SIMULATION OF GLOBE VALVE

Globe valve is basically used in fluid pipelines for controlling the flow of fluid. There will be one disc in globe valve which will be called as valve plug of the globe valve and it will control the fluid flow. It consists of one handle wheel, as shown in Figure 4.1, which used to open and close the globe valve. When handle wheel will be rotated, it will move the valve plug in upward or downward direction across the line of fluid flow. It can be seen that it has two sections. The bottom section will be connected with the inlet line and outlet line with the help of flanges and upper section of globe valve will consist with the valve plug and steam. Handle wheel and valve plug will be attached with this stem with the help of pin assemble or screw assemble. The working principle of globe valve is as follows: When the handle wheel of globe valve will be rotated in clockwise direction, steam and valve plug will move in downward direction across the fluid flow line and valve plug will be tightly located between the two valve seats. Hence there will not be any leakage of fluid through the valve once valve is closed completely (Figure 4.2).When handle wheel will be rotated in anti-clockwise direction, steam and valve plug will move in upward direction across the fluid flow line and valve will be opened from closed position and will permit the flow of fluid through the globe valve.

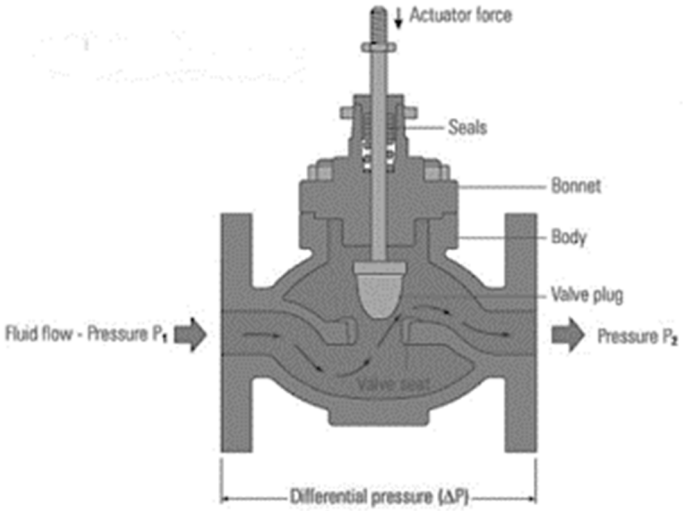

Figure 4.1: Internal structure of Globe Valve (Source: http://www.hkdivedi.com/2016/05/working-principle-of-globe-valves.html)

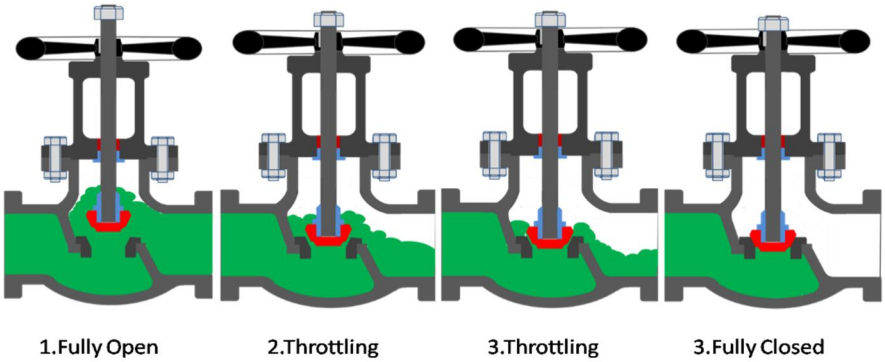

Figure 4.2. Working principle of Globe Valve
(Source: http://www.hkdivedi.com/2016/05/working-principle-of-globe-valves.html)

It can be seen from above discussion that the available flow area changes with % opening. The reduction in area leads to increase in local velocity and decrease in pressure as per Bernoulli principle. Based on local dissipation of energy, there is some permanent loss in pressure and this need to be quantified while designing the piping networks. This phenomenon is complex in nature and the present industrial practice is to use the available empirical correlations and use factor of safety in system design. The advanced tools such as computational fluid dynamics can be very useful in case of such systems to improve the reliably of design and reduce the over design which in turn helps in overall process economics.

ISSN: 2321-9653; IC Value: 45.98; SJ Impact Factor: 7.429
Volume 8 Issue XI Nov 2020- Available at www.ijraset.com

Figure 4.3 shows the velocity vectors in the globe valve at Re = 10000. It can be seen that the valve offers significant diversions in flow path. The flow once comes out of the valve, tends to travel upwards towards the top wall. The recirculation loop gets formed at the bottom side having L/D up to 2 for fully open condition and reduces to L/D of 1 for 25 % opening condition. Figure 4.4 shows the velocity magnitude in the system. It can be seen that a weak vortex forms at downstream of globe for fully open to 50% opening condition and the strength of this vortex increases with the closure of valve. The fluid hits the top side wall in case of globe valve operation. The velocity profile takes large L/D for getting restored to fully developed condition (L/D > 6). In Figure 4.5 it can be seen that the turbulent kinetic energy at top wall region is almost two orders of magnitude than the bottom side. The dissipation in valve region is higher compared to the downstream region. The turbulent intensity at the downstream is close to 88% in case of globe valve. Figure 4.6 shows the dissipation of TKE. It can be seen that globe valve do not create inhomogeneous dissipation patterns till 25% opening. The dissipation from the valve is fairly uniform and this is the reason why it is widely used flow control valve. The Ball and Gate valves are most of the times used as ON/OFF valves. Almost in all control actions, globe valves are preferred. The dissipation at the top wall downstream is in the range of 200 m2/s3 up to 50 % opening whereas as it is close to 1000 m2/s3 in case of 25% opening. Using small eddy model, the mass transfer coefficient is in the range of 0.025 m/s upto 50% opening and it is 0.038 m/s for 25% opening.

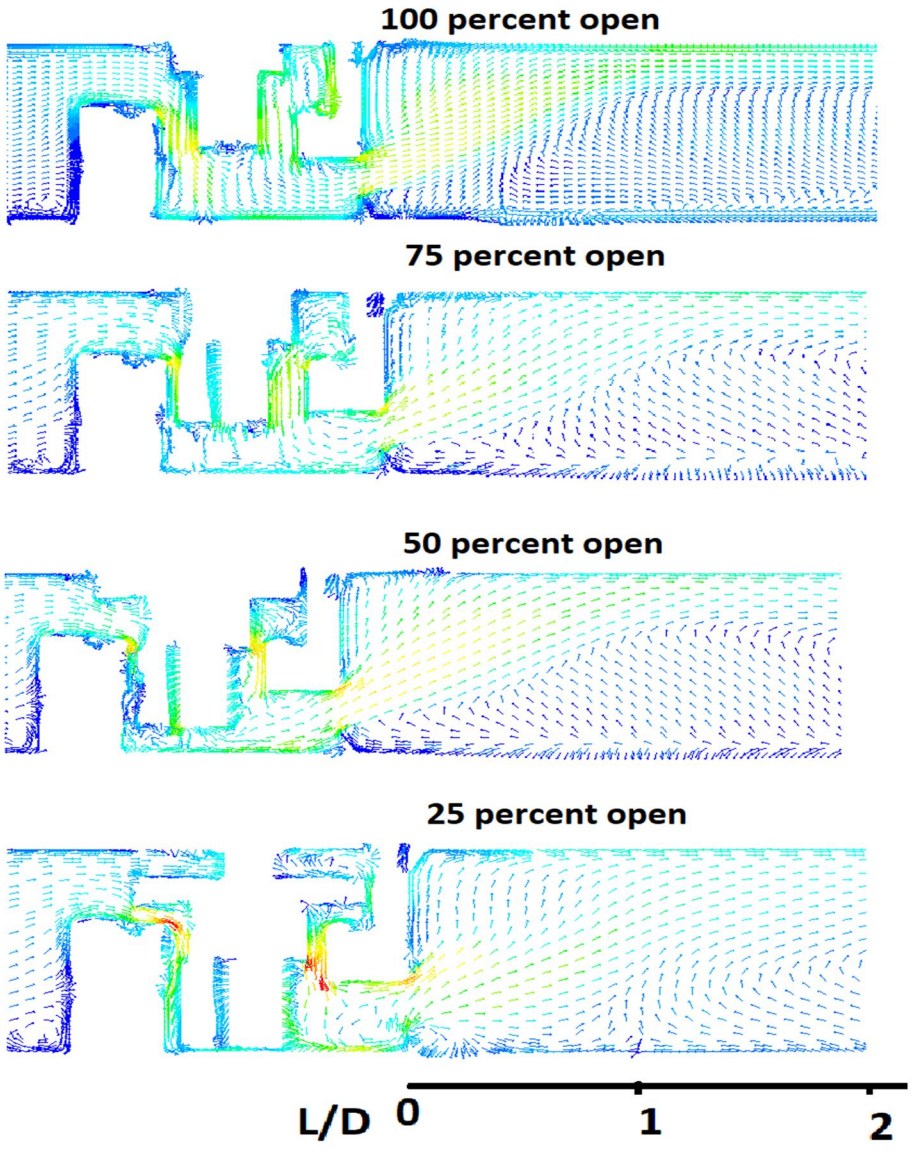

Figure 4.3: Velocity vectors in globe valve at Re = 10000

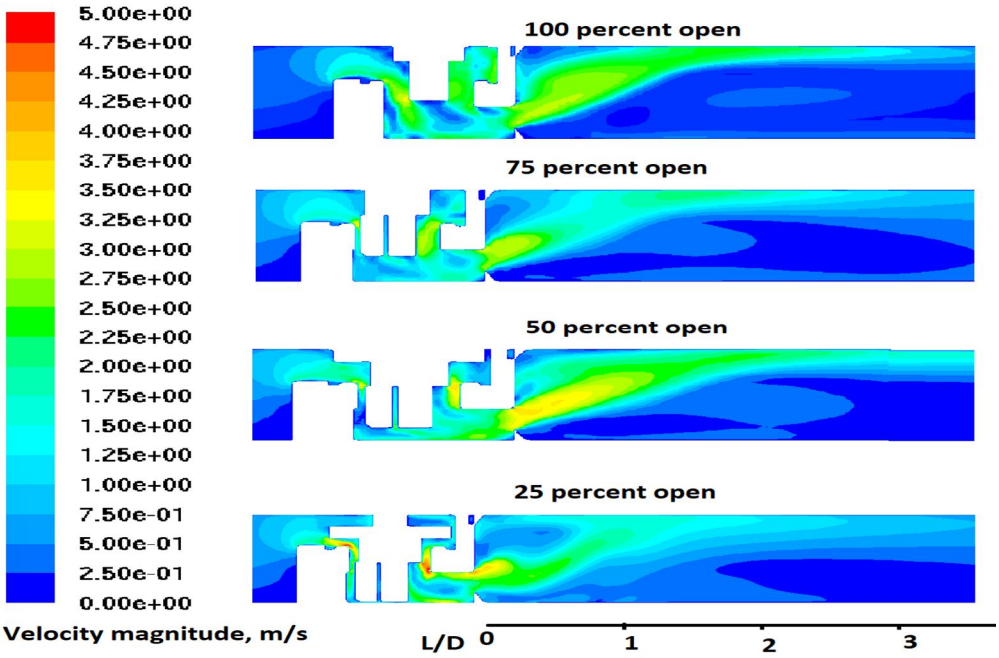

Figure 4.4 Velocity magnitudes through the globe valve

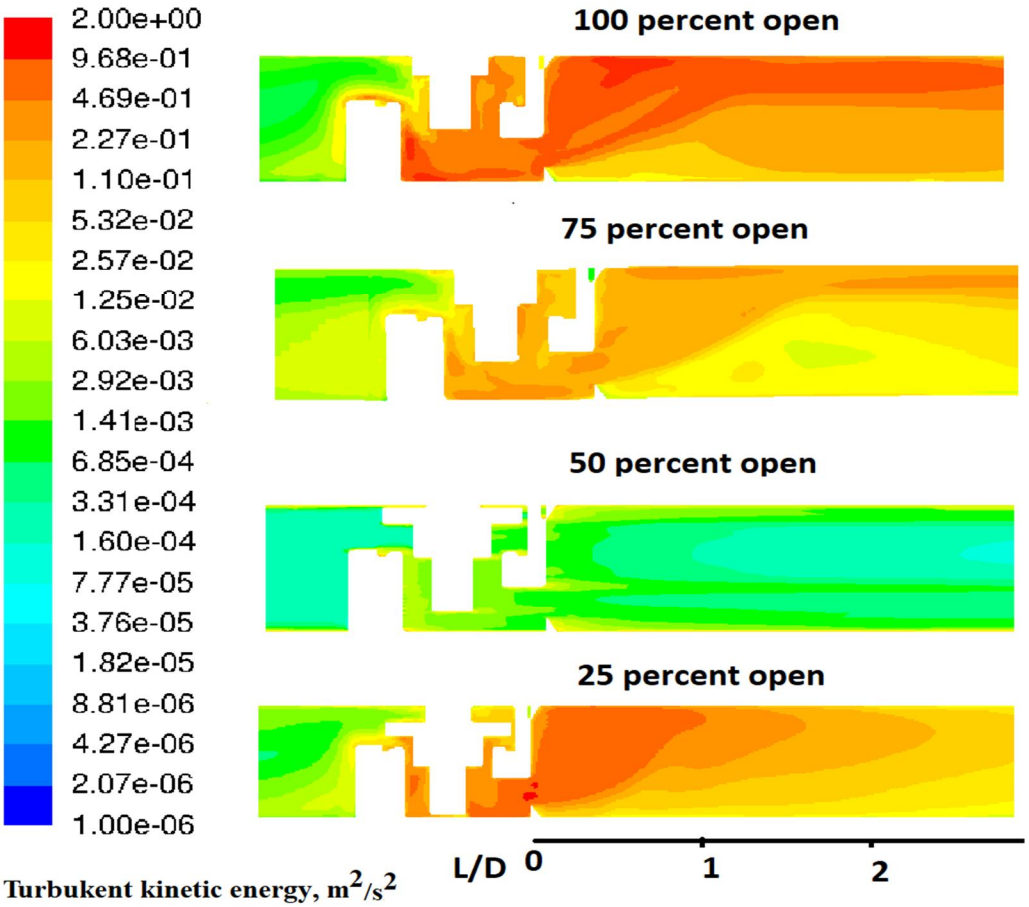

Figure 4.5. Turbulent kinetic energy through the globe valve

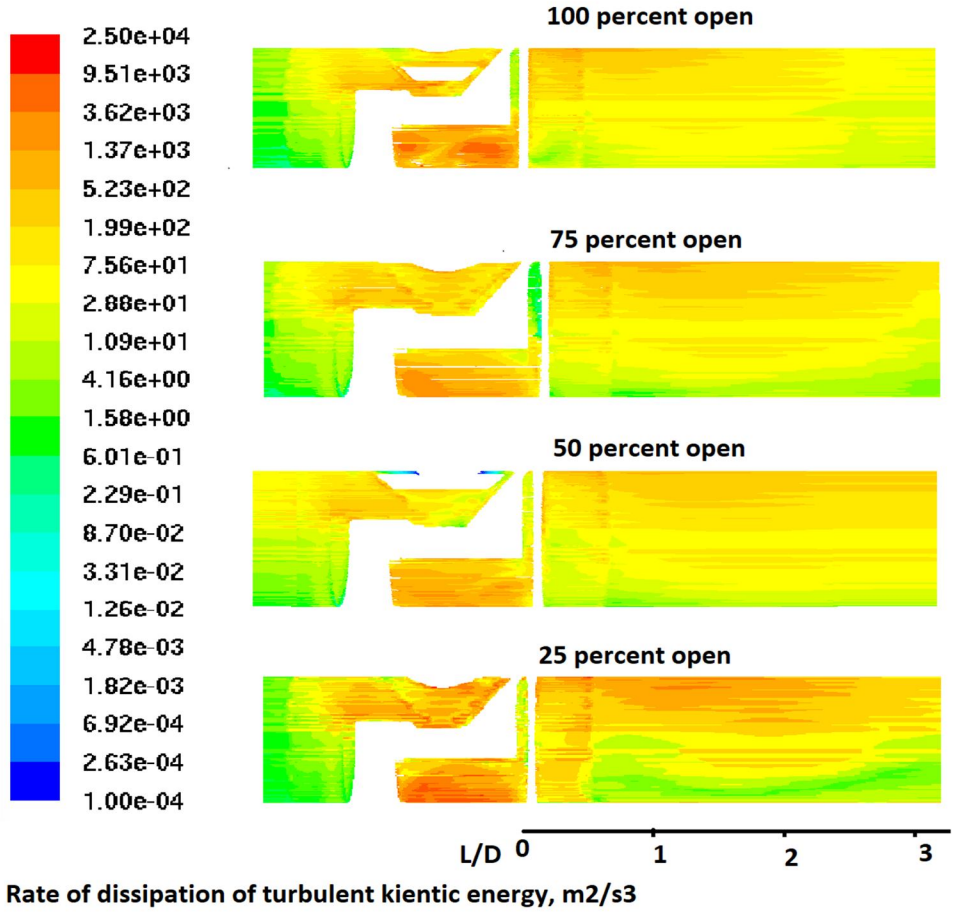

Figure 4.6 Rate of dissipation of turbulent kinetic energy

V. CFD SIMULATION OF ORIFICE METER

It is very important to measure flow rates accurately in chemical process industries. Orifice plate is most commonly used flow meter which creates pressure drop across the plate and the pressure drop is related to flow rate. Orifice plates are simple in construction, easy to install and replace and without any moving parts. Orifice flow involves flow separation, reversals and vortex formation and shedding. The schematic of flow complexity is shown in Figure 5.1. The high shear and high dissipation region downstream of orifice enhances wall mass transfer and is responsible for wall thinning (or flow assisted corrosion) in nuclear and thermal power plants.

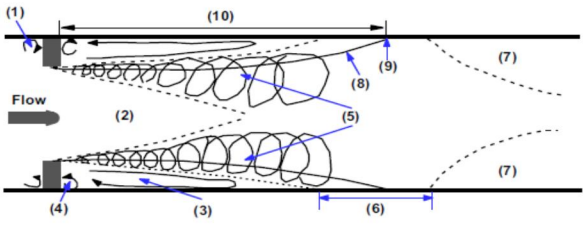

Fig. 1. Sketch of flow regions in orifice flow: (1) upstream recirculation region; (2) core region; (3) primary recirculation region; (4) secondary recirculation region; (5) axisymmetric shear-layer region; (6) reattachment region; (7) redevelopment region; (8) mean reattachment streamline; (9) mean reattachment point; (10) reattachment length x_r; the broken lines represent the imaginary boundaries of the core, shear layer, recirculation, and flow redevelopment regions; the chiral solid lines represent the vortex structures in the shear layer region.

Figure 5.1: flow regions in orifice flow (source: Shan et al., Chem. Engg. Sci. 152 (2016) 497-506)

The previous work related to orifice flow meter is listed in Appendix A. It can be seen that the pressure drop through the system depends on ratio of orifice to pipe diameter.

In this work, pipe diameter of 0.02 m and orifice diameter of 0.008 m has been used. The ratio of orifice to pipe diameter is 0.4. The total length of pipe is 1 m. Water is taken as working fluid and simulations have been carried out at three Reynolds numbers 10000, 25000 and 50000. The simulations have been carried out using Reynolds stress model and the final numbers of grid points used for simulation are 1606005 after grid independency test. The velocity profile at the downstream of orifice plate (location: L/Dpipe=1) has been used in the grid independency test. SIMPLE algorithm has been used for pressure velocity coupling and second order discretization has been used for all the variables. The pressure profile along the axial distance at different Reynolds number is shown in figure 5.2. Based on the pressure drop across the orifice plate, the coefficient of discharge has been predicted and reported in Table 5.1. It can be seen that at lower Reynolds number (Re = 10000), the Co value was in the range of 0.68 and at Re = 50000, Co value is 0.61. The results are in agreement with literature data which is shown in Figure 5.3.

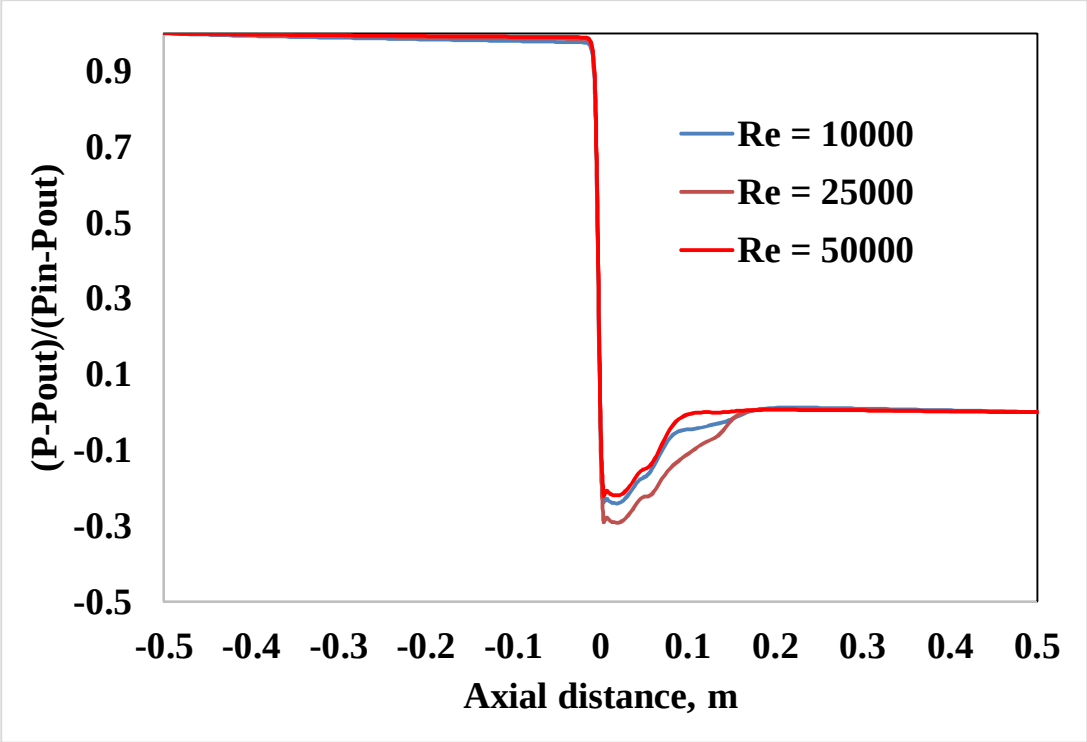

Figure 5.2: Pressure profile through orifice

The rate of dissipation of turbulent kinetic energy and pressure drop has been reported in Table 5.1. Figure 5.4 shows the velocity profile through the orifice. It can be seen that complex flow patterns get created downstream of orifice plate as seen in Figure 5.1. Figure 5.5 shows the turbulent kinetic energy at different Reynolds number. It can be seen that change in Reynolds number from 10000 to 50000, turbulent kinetic energy changes from 0.8 to 20 m^2/s^2. Figure 5.6 shows the profile of rate of dissipation of turbulent kinetic energy. With increase in Re, the dissipation rate increases exponentially. It can be seen that with increase in Re, high dissipation is also observed on pipe wall from L/D = 1 to L/D = 4, downstream of orifice. The mass transfer coefficient at wall is proportional to square root of dissipation rate as per the analogy of heat, mass and momentum transfer. One can use small eddy model to predict the mass transfer at wall.

Table 5.1: CFD predictions in orifice flow at different Reynolds number

Re	V	Q	ε (CFD)	ΔP	C_O
(-)	m/s	m^3/s	m^2/s^3	Pa	(-)
10000	0.53	1.67E-04	3.31	580.0	0.68
25000	1.325	4.16E-04	57.84	4220.0	0.63
50000	2.65	8.33E-04	339.78	17875.0	0.61

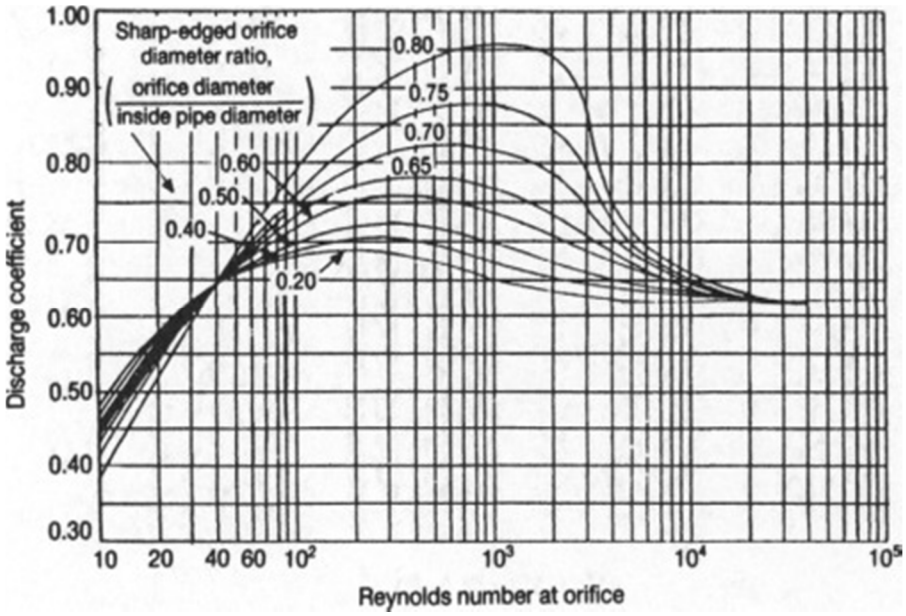

Figure 5.3 Orifice discharge coefficient as a function of diameter ratio and Reynolds number
(Source:https://www.sciencedirect.com/topics/engineering/orifice-meter)

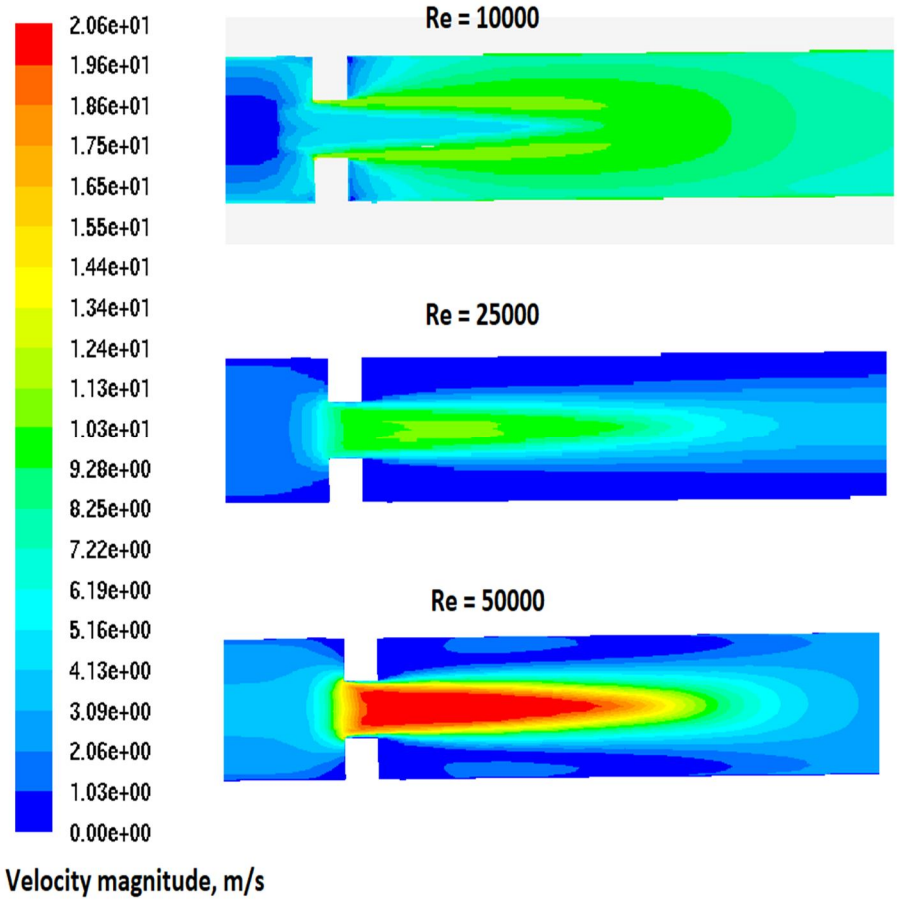

Figure 2.4: Velocity profile through orifice at different Reynolds number

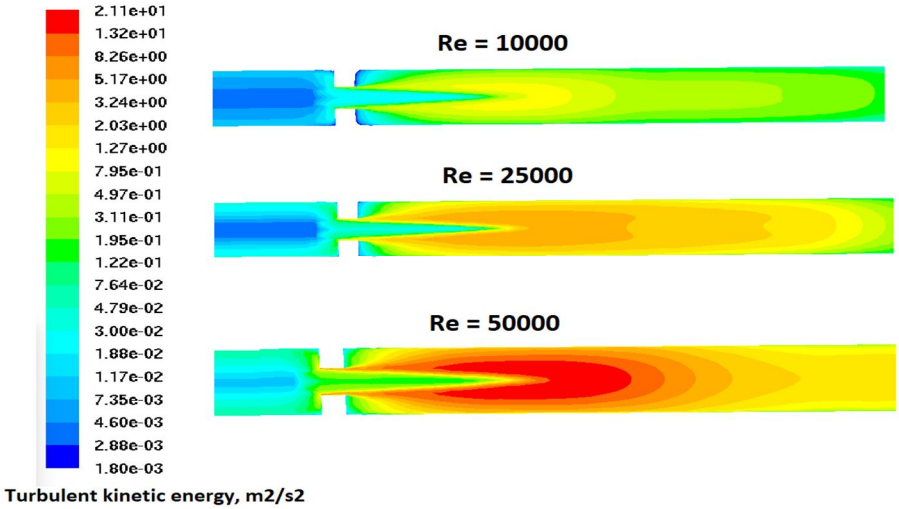

Figure 5.5. Turbulent kinetic energy through orifice at different Reynolds number

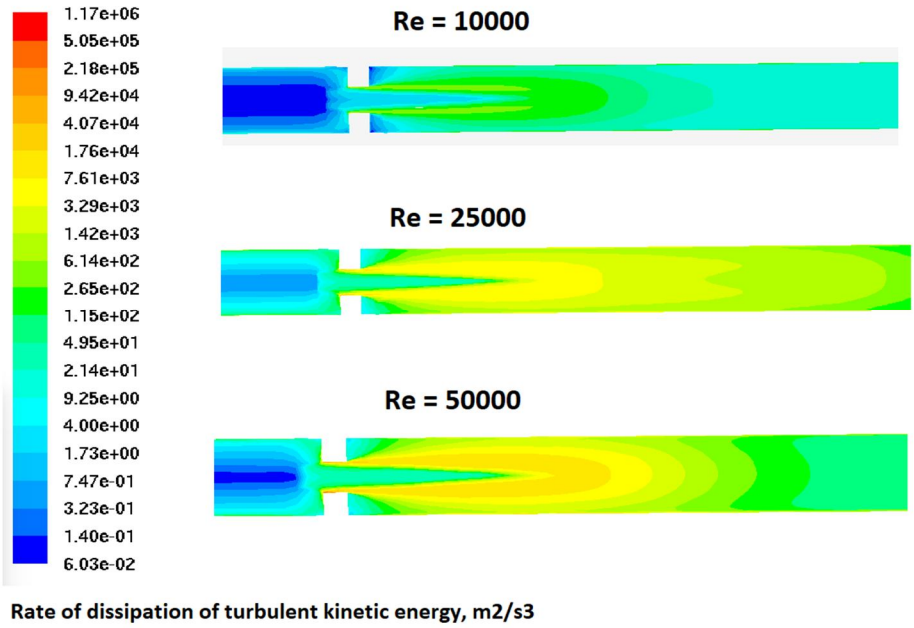

Figure 5.6. Rate of dissipation of turbulent kinetic energy through orifice at different Reynolds number

VI. CONCLUSION

In this article, CFD analysis has been carried out of various valves and pipe fittings such as orifice, ball valve, gate valve and globe valve. CFD is an important tool to probe inside the fluid systems and understand the hydraulic performance of the systems. CFD is capable to predict the exact physics of the flow. The orifice simulations show that CFD can predict pressure velocity conversion very well and it also predict the high shear/dissipation regions downstream and using theories of turbulence and analogies of heat/mass transfer, the wear rate of piping systems can be predicted. The flow simulations of ball, gate and globe valve show that the turbulence in the system changes exponentially with valve closure and the location of wear also depends on the % opening as well as the magnitude of wear which is accounted through the wall side mass transfer coefficient. It is necessary to avoid the high dissipation regions as these piping systems are in operation continuously without maintenance downtime and wear can lead to leakage or rupture of piping system. This may lead to accidental scenarios. The quantification of wear rate can help us to identify the replacement frequency of such pipe fittings and the connecting piping units.

REFERENCES

[1] Shirazi N.T., Azizyan G.R., Akbari G.H., CFD analysis of the ball valve performance in presence of cavitation (2012) Life Science Journal, 9(4),1460-1467
[2] Moujaes S.F., Jagan R. 3D CFD predictions and experimental comparisons of pressure drop in a ball valve at different partial openings in turbulent flow 2008 Journal of Energy Engineering 134 (1), 24-28.
[3] Augusto P.E.D., CristianiniM.Using computational fluid dynamics (CFD) for evaluation of fluid flow through a gate Valve, (2012) International Journal of Food Engineering, 8, 4-21
[4] Choudhary S., Rana S.C. Numerical study of partially closed knife gate valve using rans and les approaches, (2017) International Journal of Mechanical Engineering and Technology, 8(5), 432-445.
[5] Tang Y., Tang L., Liu E., 3D simulation and transient model for regulating period of gate valve, (2012) Journal of Drainage and Irrigation Machinery Engineering, 30(2), 219-224
[6] Lin Z., Ruan X.-D., Zhu Z.-C., Fu X. Three-dimensional numerical investigation of solid particle erosion in gate valves, (2014) Proceedings of the Institution of Mechanical Engineers, Part C: Journal of Mechanical Engineering Science, 228 (10), 1670-1679

1) Appendix A : Literature survey related to orifice flow

Author	Pipe diameter (mm)	beta	Working fluid	Flow condition
Shah et al. (2012)	12.3, 25.4 and 50.8	0.08 to 0.5	Water and air	0.3 to 11.3 m/s
Ho and Leung (1985)	25.4	0.274,0.36,0.448	water	100-1000
Nail (1991)	25.4	0.5	Air	18400
Morrison et.al (1993)	50.8	0.5	Air	91100
Smith et al (2008)	25.4	0.5,0.6,0.8	Air	18400
Naveenjiet al. (2010)	50,100,200	0.4-0.8	Non-Newtonian fluid (prepared with varyng concentration of salt)	100-10000
Oliveira et al (2010)	100	0.1-0.6	Water	$4000\text{-}10^6$

2) Appendix B: Governing equations in CFD

Computational fluid dynamics (CFD) is widely used for understanding the turbulent transport of mass, momentum and heat in chemical process equipment. Understanding of mixing and heat, mass transport rates in the reactors is essential for the reliable and efficient design. To achieve this, information regarding the velocity, pressure, distribution of kinetic energy and local dissipation is required in time as well as space domain.

The equations of change for a three dimensional incompressible system can be represented in the following form (Pope, 2000):

$$\frac{\partial u_i}{\partial x_i} = 0 \qquad \text{(B.1)}$$

$$\rho \frac{\partial u_i}{\partial t} + \rho u_j \frac{\partial u_i}{\partial x_j} = -\frac{\partial p}{\partial x_i} + \frac{\partial}{\partial x_j}\left(\mu \frac{\partial u_i}{\partial x_j} \right) \qquad \text{(B.2)}$$

The equation (4.1) and (4.2) are instantaneous equations and will require very high computational power to solve as one need to have very fine mesh size (less than Kolmogorov length scale), hence for engineering purpose, these equations are time averaged and the modified set of equations are solved on coarser mesh and the effect of turbulence is modelled through other set of transport equations which quantify turbulent viscosity. The turbulent viscosity is a hypothetical concept which is used to close the system of equations as the time averaging process leads to an additional term known as Reynolds stress. Equation (4.3) and (4.4) are time averaged equations of continuity and motion.

$$\frac{\partial \langle u_i \rangle}{\partial x_i} = 0 \qquad \text{(B.3)}$$

$$\rho \frac{\partial \langle u_i \rangle}{\partial t} + \rho \langle u_j \rangle \frac{\partial \langle u_i \rangle}{\partial x_j} = -\frac{\partial \langle p \rangle}{\partial x_i} + \frac{\partial}{\partial x_j}\left(\mu \frac{\partial \langle u_i \rangle}{\partial x_j} - \rho \langle u_i' u_j' \rangle \right) \qquad \text{(B.4)}$$

The Reynolds stresses ($-\rho \partial \langle u_i' u_j' \rangle / \partial x_j$) in Equation (4.4) arises out of ensemble-averaging procedure are modelled according to the Boussinesq hypothesis and given by:

$$-\rho \langle u_i' u_j' \rangle = \frac{2}{3} k \rho \delta_{ij} - \mu_t \left(\frac{\partial \langle u_i \rangle}{\partial x_j} + \frac{\partial \langle u_j \rangle}{\partial x_i} \right) \qquad \text{(B.5)}$$

ISSN: 2321-9653; IC Value: 45.98; SJ Impact Factor: 7.429
Volume 8 Issue XI Nov 2020- Available at www.ijraset.com

a) Standard k-ε model

In order to close the system of equations μ_t has been formulated in many ways in the literature in terms of zero, one and two equation models. The most popular is the two equation model where μ_t is estimated from turbulent length and time scales. In the case of standard *k-ε* model, μ_t is estimated using turbulent kinetic energy (*k*) and rate of dissipation of turbulent kinetic energy (*ε*).

$$\mu_t = C_\mu \rho \frac{k^2}{\varepsilon} \tag{B.6}$$

The values of *k* and *ε* are obtained by solving their transport equations (Launder and Spalding, 1972). However, the exact *k* and*ε* equations cannot be solved directly, as they contain triple correlations of fluctuating velocity, or ensemble-averaging of gradients of fluctuating velocities. These terms cannot be estimated directly and need modelling. The abovementioned modelling of *k* and *ε* equations result into five turbulence parameters $C_\mu, C_{\varepsilon 1}, C_{\varepsilon 2}, \sigma_k$ and σ_ε. These parameters have been estimated from studies in simple flows. In the log-law region of the boundary layer, experimentally it has been found that the turbulence production and the dissipation terms are much larger than the other terms. Turbulence in this region is considered to be in local equilibrium. Neglecting transport and production in this flow, value of C_μ = 0.09 has been obtained. For the value of $C_{\varepsilon 2}$, experiments have been carried out in decaying grid turbulence. Turbulence is generated when free flow goes through a grid which generates mean flow gradients and in turn via the production term generates turbulence. Sufficiently far downstream, the velocity gradients are zero and hence the production and dissipation terms are zero in contrast to log-law region in the boundary layer. The turbulent diffusion term is also negligible. The balance of turbulence convection and dissipation gives $C_{\varepsilon 2}$=1.92. The constant $C_{\varepsilon 1}$ is obtained by looking at the dissipation rate equation in the log-region of boundary layer. The turbulent diffusion is not negligible in this case unlike *k* equation. The simplifications of ε□ equation using velocity profiles in log law region and the numerical solution of these equations give $C_{\varepsilon 1}$ =1.44, σ_k and σ_ε = 1.0 and 1.3 respectively.

Further, the modelling of transport equations for *k* and *ε* pose the difficulties to account for streamline curvature, rotational strains, and the other body-force effects. The standard k-e model equations are given below:

$$\left\{\rho\frac{\partial k}{\partial t}\right\}+\left\{\rho\langle u_k\rangle\frac{\partial k}{\partial x_k}\right\}=\left\{\tau_{ij}\frac{\partial\langle u_i\rangle}{\partial x_j}\right\}+\left\{\frac{\partial}{\partial x_k}\left(\frac{\mu_t}{\sigma_k}\frac{\partial k}{\partial x_k}\right)\right\}+\left\{\frac{\partial}{\partial x_k}\left(\mu\frac{\partial k}{\partial x_k}\right)\right\}+\{-\rho\varepsilon\} \tag{B.7}$$

$$\left\{\rho\frac{\partial \varepsilon}{\partial t}\right\}+\left\{\rho\langle u_j\rangle\frac{\partial \varepsilon}{\partial x_j}\right\}=\left\{\rho C_{\varepsilon 1}\frac{\varepsilon}{k}\tau_{ij}\frac{\partial\langle u_i\rangle}{\partial x_j}\right\}+\left\{\frac{\partial}{\partial x_j}\left(\frac{\mu_t}{\sigma_\varepsilon}\frac{\partial \varepsilon}{\partial x_j}\right)\right\}+\left\{\frac{\partial}{\partial x_j}\left(\mu\frac{\partial \varepsilon}{\partial x_j}\right)\right\}+\left\{-C_{\varepsilon 2}\rho\frac{\varepsilon^2}{k}\right\} \tag{B.8}$$

b) SST k-ω model

Large numerical problems are associated with *k-ε* model in the region of low turbulence where both *k* as well as*ε* tend to zero. The destruction term in *ε* equation involves ε^2/k. To avoid such problems, *k-ω* models have been developed where $\omega = \varepsilon/k$ (specific rate of dissipation). When k tends to zero, in *ω* equation turbulent diffusion term simply goes to zero and production term in *ω* equation does not include *k*. The standard *k-ω* model was proposed by Wilcox (1994).

One modification of standard *k-ω* model is SST *k-ω* model (Menter, 1994). The SST model combined the robustness of the *k-ω* turbulence model near walls with the capabilities of the *k–ε* model away from the walls (also removing the strong sensitivity to variations in far field *ω* boundary conditions. This model also includes the fact that the shear stress in a boundary layer is proportional to the turbulent kinetic energy. The transport equations for SST *k-ω* model are given below. The SST *k-ω* has been found to perform very well for transitional and re-circulating flows.

$$\frac{D\rho k}{Dt}=\tau_{ij}\frac{\partial u_i}{\partial x_j}-\beta^*\rho\omega k+\frac{\partial}{\partial x_j}\left[\left(\mu+\frac{\mu_t}{\sigma_k}\right)\frac{\partial k}{\partial x_j}\right] \tag{B.9}$$

$$\frac{D\rho\omega}{Dt}=\frac{\gamma\rho}{\mu_t}\tau_{ij}\frac{\partial u_i}{\partial x_j}-\beta\rho\omega^2+\frac{\partial}{\partial x_j}\left[\left(\mu+\frac{\mu_t}{\sigma_\omega}\right)\frac{\partial\omega}{\partial x_j}\right]+2(1-F_1)\frac{\rho}{\sigma_{\omega2}\omega}\frac{\partial k}{\partial x_j}\frac{\partial\omega}{\partial x_j}$$

$$\mu_t=\frac{\rho a_1 k}{\max(a_1\omega,\Omega F_2)}\qquad F_1=\tanh\left(\Gamma^4\right)\qquad \Gamma=\min\left(\left[\max\left(\frac{\sqrt{k}}{\beta^*\omega d},\frac{500\mu}{\rho\omega d^2}\right)\right],\frac{4\rho k}{\sigma_{\omega2}CD_{k\omega}d^2}\right) \tag{B.10}$$

$$CD_{k\omega}=\max\left(\frac{2\rho}{\sigma_{\omega2}\omega}\frac{\partial k}{\partial x_j}\frac{\partial\omega}{\partial x_j},10^{-20}\right)\qquad F_2=\tanh\left(\Pi^2\right)\qquad \Pi=\max\left(\frac{2\sqrt{k}}{\beta^*\omega d},\frac{500\mu}{\rho\omega d^2}\right)$$

$$\begin{aligned}\gamma&=F_1\gamma_1+(1-F_1)\gamma_2\\ \sigma_k&=F_1\sigma_{k1}+(1-F_1)\sigma_{k2}\\ \sigma_\omega&=F_1\sigma_{\omega1}+(1-F_1)\sigma_{\omega2}\\ \beta&=F_1\beta_1+(1-F_1)\beta_2\end{aligned} \tag{B.11}$$

c) Reynolds stress model (RSM)

It is clear that the standard k - ε model inherently fails to predict properly the anisotropic flow situations **(**Reynolds, 1987, Launder 1990, Hanjalic 1994). Further, the modelling of transport equations for k and ε clearly brings out the difficulties to account for streamline curvature, rotational strains, and the other body-force effects. Reynolds stress model, in theory, can circumvent all the above mentioned deficiencies and also it has an ability to predict more accurately each individual stress. A Reynolds stress model solves six equations for the Reynolds stress tensor and another equation for the dissipation rate. The equation of turbulent stresses contains the terms, namely pressure strain rate (which contains fluctuating pressure velocity gradients) and the flux of Reynolds stresses. In addition to the modelling of the terms in the turbulent energy dissipation rate equation, these terms need to be modelled accurately. Therefore, though RSM takes into consideration the transport of turbulent stresses, its parameters are not universal (i.e. model needs to be calibrated for different types of flows). Further, the extended system often has difficulties to produce converged solutions and thus it is computationally expensive. The Reynolds stress model equation (4.12) is solved in addition to dissipation rate equation as listed in *k-ε* model (Equation 4.6).

$$\left\{\rho\frac{\partial\tau_{ij}}{\partial t}\right\}+\left\{\rho\langle u_k\rangle\frac{\partial\tau_{ij}}{\partial x_k}\right\}=\left\{-\rho\left(\tau_{ik}\frac{\partial\langle u_j\rangle}{\partial x_k}+\tau_{jk}\frac{\partial\langle u_i\rangle}{\partial x_k}\right)\right\}+\left\{\frac{\partial}{\partial x_k}\left(\frac{\mu_t}{\sigma_k}\frac{\partial\tau_{ij}}{\partial x_k}\right)\right\}+\left\{\frac{\partial}{\partial x_k}\left(\mu\frac{\partial\tau_{ij}}{\partial x_k}\right)\right\}+\left\{-\frac{2}{3}\varepsilon\delta_{ij}\right\}+\left\{\Pi_{ij}\right\} \tag{B.12}$$

d) Large eddy simulation

Spatial filtering is applied in large eddy simulation. All the scales, larger than the filter size are resolved and the remaining is modelled. When the Navier-Stokes equations for constant density (incompressible flow) are filtered, one obtains a set of equations very similar to the RANS equations:

$$\nabla.\bar{u}=0 \tag{B.13}$$

$$\frac{\partial\bar{u}}{\partial t}+\nabla.(\overline{uu})=-\frac{1}{\rho}\nabla\bar{p}+\nu\nabla^2\bar{u} \tag{B.14}$$

Since the continuity equation is linear, filtering does not change it significantly. The continuity equation Eq. (1) is used in the momentum equation Eq. (2) to reformulate the advective term into its conservative form. The nonlinear transport term in the filtered equation can be developed as:

$$\overline{uu}=\overline{(\bar{u}+u')(\bar{u}+u')} \tag{B.15}$$

$$\bar{\bar{u}}\bar{\bar{u}}+\overline{\bar{u}u'}+\overline{u'\bar{u}}+\overline{u'u'} \tag{B.16}$$

In time averaging the terms (2) and (3) vanish, but while using volume averaging this is no longer true. Let us introduce the subgrid scale (SGS) stresses, τ_{ij}, as:

$$\tau=\overline{uu}-\bar{u}\bar{u} \tag{B.17}$$

Rewriting the filtered Navier-Stokes equation Eq. (2) as:

$$\frac{\partial \bar{u}}{\partial t} + \nabla.(\overline{\bar{u}\bar{u}}) = -\frac{1}{\rho}\nabla \bar{p} + \nu\nabla^2 \bar{u} - \nabla.\tau \tag{B.18}$$

$$\tau = \overline{uu} - \overline{\bar{u}\bar{u}} \tag{B.19}$$

$$\underbrace{\overline{\bar{u}\bar{u}} - \overline{\bar{u}\bar{u}}}_{L_{ij}} + \underbrace{\overline{\bar{u}u'} + \overline{\bar{u}u'}}_{C_{ij}} + \underbrace{\overline{u'u'}}_{R_{ij}} \tag{B.20}$$

It is only important to note that τ includes the SGS component u' of the velocity vector u and hence it is unknown. Expressions for τ need to be formulated either by deriving prognostic partial differential equations for all its components or by relating τ in an algebraic way directly to the grid scale (GS) velocity vector $\bar{u}$ .The main role of the subgrid-scale (SGS) model is to remove energy from the resolved scales. In LES, the small dissipative scales are not *resolved* accurately, so the SGS model is needed to represent the kinetic energy losses due to the viscous forces. Thus, the SGS models do not attempt to produce the SGS stresses accurately, but only to account their effect in a statistical sense. In this work, one equation dynamics subgridscale model has been used.
The transport equation for the subgrid kinetic energy E_{sgs} is given as:

$$\frac{\partial E_{sgs}}{\partial t} + \frac{\partial E_{sgs}\bar{u}_j}{\partial x_j} = -\frac{\partial}{\partial x_j}\left(\frac{1}{2}\overline{u_i u_j u_j} - E_{kin}\bar{u}_j - \frac{1}{\rho}\left(\overline{uP}_j - \bar{u}_j\bar{P}\right) - \tau_{ij}\bar{u}_i\right)$$
$$+\nu\frac{\partial^2 E_{sgs}}{\partial x_j{}^2} - \nu\left(\overline{\frac{\partial u_i}{\partial x_j}\frac{\partial u_i}{\partial x_j}} - \frac{\partial \bar{u}_i}{\partial x_j}\frac{\partial \bar{u}_i}{\partial x_j}\right) - \tau_{ij}\frac{\partial \bar{u}_i}{\partial x_j} \tag{B.21}$$

The simulations have been carried out in 0.2 m wide x 0.0285 m deep x 2 m long water channel at Re = 4000. The Reynolds number has been calculated using the boundary layer thickness (δ) as the length scale (using the same procedure $\left(Re = 2\delta u\rho/\mu\right)$ as defined by Meek (1972)) In case of LES modelling, one equation dynamic sub grid scale kinetic energy model has been used for closure (Kim et al., 1997).

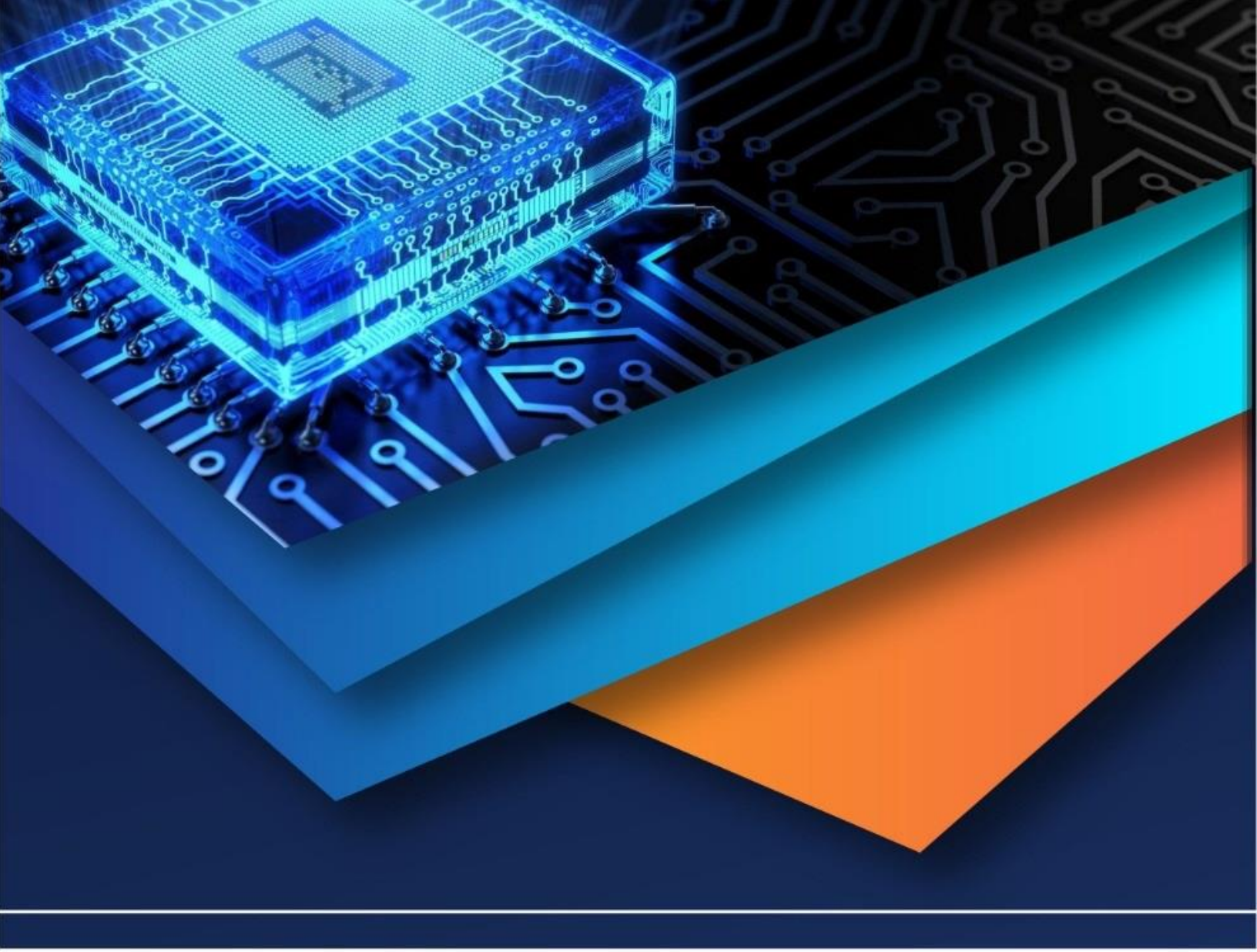

10.22214/IJRASET

45.98

IMPACT FACTOR: 7.129

IMPACT FACTOR: 7.429

INTERNATIONAL JOURNAL FOR RESEARCH

IN APPLIED SCIENCE & ENGINEERING TECHNOLOGY